Centimeter-Accurate UAV Navigation with Cellular Signals

Joe J. Khalife, Souradeep Bhattacharya, and Zaher M. Kassas
University of California, Riverside

BIOGRAPHIES

Joe J. Khalife is a Ph.D. Candidate in the Department of Electrical and Computer Engineering at the University of California, Riverside (UCR) and a member of the Autonomous Systems Perception, Intelligence, and Navigation (ASPIN) Laboratory. He received a B.E. in Electrical Engineering and an M.S. in Computer Engineering from the Lebanese American University (LAU). His research interests include opportunistic navigation, autonomous vehicles, and software-defined radio.

Souradeep Bhattacharya received a B.S. in Bioengineering and a B.S. in Electrical Engineering from UCR. He was a member of ASPIN Laboratory at UCR where his research interests included robotics, heterogeneous computing, artificial intelligence, and machine learning.

Zaher (Zak) M. Kassas is an assistant professor at UCR and director of the ASPIN Laboratory. He received a B.E. in Electrical Engineering from LAU, an M.S. in Electrical and Computer Engineering from The Ohio State University, and an M.S.E. in Aerospace Engineering and a Ph.D. in Electrical and Computer Engineering from The University of Texas at Austin. In 2018, he received the National Science Foundation (NSF) Faculty Early Career Development Program (CAREER) Award. His research interests include cyber-physical systems, estimation theory, navigation systems, autonomous vehicles, and intelligent transportation systems.

ABSTRACT

This paper proposes a framework for unmanned aerial vehicle (UAV) navigation using carrier phase differential cellular (CD-cellular) measurements. The framework requires no prior knowledge of the UAV's position and achieves centimeter-level position accuracy. A batch weighted nonlinear least-squares estimator is developed to solve for the integer ambiguities and an extended Kalman filter is formulated to initialize the batch estimator. Monte Carlo simulations are presented to characterize the performance of the proposed framework as a function of the total number of hearable cellular base transceiver stations (BTSs) and the size of the batch estimator. Experimental results are presented demonstrating a UAV navigating exclusively using the proposed framework over a 1.72 km trajectory completed in 3 minutes with 62.11 cm root mean-square error (RMSE).

I. INTRODUCTION

The potential of signals of opportunity (SOPs) (e.g., AM/FM radio [1, 2], iridium satellite signals [3, 4], WiFi [5, 6], and cellular [7–10]) as alternative navigation sources to global navigation satellite signal (GNSS) has been the subject of extensive research recently. Navigation with SOPs has been demonstrated on ground vehicles and unmanned aerial vehicles (UAVs), achieving a positioning accuracy ranging from meters to tens of meters, with the latter accuracy corresponding to ground vehicles in deep urban canyons with severe multipath conditions [11–14]. Cellular SOPs possess particularly desirable attributes for navigation. First, when fused with GNSS signals, cellular signals have been shown to significantly reduce the vertical dilution of precision (VDOP) [14–16]. Second, cellular signals can be used as an aiding source instead of GNSS signals to aid an inertial navigation system [17–20]. Third, cellular signals can be fused with lidar, significantly reducing the computational burden associated with maintaining the lidar's point cloud by using only a very small fraction of these points, while achieving lane-level accuracy on ground vehicles [21, 22].

Cellular signals are typically transmitted at a very high power, in several bands, and in several channels within each band, which aggregates to tens of megahertz in bandwidth on the radio frequency (RF) spectrum. Therefore, jamming or spoofing all cellular signals simultaneously requires sophisticated hardware and impractically large power,

Preprint of the 2018 ION GNSS+ Conference
Miami, FL, September 24–28, 2018

which is practically impossible. If only a few bands or channels become the target of a jamming or spoofing attack, a cellular navigation receiver may switch to a different band or channel, maintaining the capability of producing a reliable navigation solution at all time. Software-defined radios (SDRs) enable the development of cellular SOP navigation receivers with such capabilities [23–26].

Besides cellular SOPs' attractive attributes against jamming and spoofing attacks, they may yield a precise navigation solution if one exploits their carrier phase. This technique is well known in GNSS and sub-meter-level (centimeter to decimeter) is common in carrier phase differential GNSS (CDGNSS), also known as real-time kinematic (RTK) [27, 28]. The first study of cellular carrier phase-based navigation was conducted in [29], in which the received carrier phase of cellular code-division multiple access (CDMA) signals was exploited to produce sub-meter-level accurate navigation solutions on a UAV. The paper proposed two navigation frameworks: the first is based on carrier phase differential measurements, requiring an additional base receiver, and the second leveraged the relative frequency stability of cellular base transceiver station (BTS) clocks, alleviating the need of such base receiver. Although the second approach is attractive for single UAV navigation, it may not yield sub-meter-level navigation accuracy if the relative drift between BTS clocks is not small enough, a requirement that is not necessarily met in all cellular networks.

While the first approach is robust against poor BTS synchronization, one may argue that the need for a base receiver could pose a practical limitation. However, considering the need for a resilient and accurate position, navigation, and timing (PNT) alternative to GNSS in future UAV applications (e.g., package delivery, environmental monitoring, search and rescue, etc.), installing a dedicated carrier phase differential cellular (CD-cellular) network is lucrative. Recent advances in SDRs and embedded computing pave the road to making such networks for precise UAV navigation a reality.

This paper makes four contributions. First, a CD-cellular navigation framework is developed for cellular signals and a method for resolving carrier phase ambiguities is discussed. Second, the proposed framework is evaluated through Monte Carlo simulations. Third, important design considerations of a practical CD-cellular navigation network and their effect on the navigation performance are studied, namely: 1) the number of bases needed to cover a given cellular SOP environment and the base placement that maximizes availability, 2) communication requirements and synchronization of CD-cellular measurements shared between the bases and navigating UAVs, and 3) hardware and software consideration for real-time implementation. Fourth, experimental results are presented demonstrating a UAV navigating exclusively with CD-cellular measurements for 3 minutes and over a 1.7 km trajectory with a position root-mean squared error (RMSE) of 62.11 centimeters.

The rest of the paper is organized as follows. Section II describes the carrier phase measurement model and the pseudorange model parameterized by the receiver and BTS states. Section III describes the CD-cellular navigation framework. Section IV provides Monte Carlo simulation results to assess the performance of the proposed framework. Section V provides a preliminary CD-cellular network design analysis and software and hardware considerations for real-time implementation of a CD-cellular network. SectionVI shows experimental results demonstrating centimeter-level-accurate UAV navigation via the proposed CD-cellular framework. Concluding remarks are given in Section VII.

II. MODEL DESCRIPTION

A. UAV-MOUNTED RECEIVER DYNAMICS MODEL

The navigating UAV-mounted receiver state consists of its unknown two-dimensional (2–D) position $\boldsymbol{r}_{r_{\mathrm{U}}} \triangleq [x_{r_{\mathrm{U}}}, y_{r_{\mathrm{U}}}]^{\mathsf{T}}$ and velocity $\dot{\boldsymbol{r}}_{r_{\mathrm{U}}}$. An altimeter may be used to estimate the UAV's altitude. The subsequent analysis may be readily extended to 3–D; however, the vertical position estimate will suffer from large uncertainties due to the poor vertical diversity of cellular SOPs. Hence, the state vector of the UAV-mounted receiver is given by $\boldsymbol{x}_{r_{\mathrm{U}}} = \left[\boldsymbol{r}_{r_{\mathrm{U}}}^{\mathsf{T}}, \dot{\boldsymbol{r}}_{r_{\mathrm{U}}}^{\mathsf{T}}\right]^{\mathsf{T}}$. The navigating UAV's position $\boldsymbol{r}_{r_{\mathrm{U}}}$ and velocity $\dot{\boldsymbol{r}}_{r_{\mathrm{U}}}$ will be assumed to evolve according to a continuous-time velocity random walk model [30]. Therefore, the navigating UAV dynamics is modeled according to the discretized model

$$\boldsymbol{x}_{r_{\mathrm{U}}}(k+1) = \mathbf{F}_{r_{\mathrm{U}}}\, \boldsymbol{x}_{r_{\mathrm{U}}}(k) + \boldsymbol{w}_{r_{\mathrm{U}}}(k), \quad k = 0, 1, 2, \ldots, \tag{1}$$

where $\boldsymbol{w}_{r_{\mathrm{U}}}$ is a discrete-time zero-mean white noise sequence with covariance $\mathbf{Q}_{r_{\mathrm{U}}}$, with

$$\mathbf{F}_{r_{\mathrm{U}}} = \begin{bmatrix} \mathbf{I}_{2\times 2} & T\mathbf{I}_{2\times 2} \\ \mathbf{0}_{2\times 2} & \mathbf{I}_{2\times 2} \end{bmatrix}, \qquad \mathbf{Q}_{\mathbf{r}_{\mathrm{U}}} = \begin{bmatrix} \tilde{q}_x \frac{T^3}{3} & 0 & \tilde{q}_x \frac{T^2}{2} & 0 \\ 0 & \tilde{q}_y \frac{T^3}{3} & 0 & \tilde{q}_y \frac{T^2}{2} \\ \tilde{q}_x \frac{T^2}{2} & 0 & \tilde{q}_x T & 0 \\ 0 & \tilde{q}_y \frac{T^2}{2} & 0 & \tilde{q}_y T \end{bmatrix},$$

where T is the sampling time and $\tilde{q}_x$ and $\tilde{q}_y$ are the power spectral densities of the continuous-time x– and y–acceleration noise, respectively.

B. CELLULAR CARRIER PHASE OBSERVATION MODEL

In cellular systems, several known signals may be transmitted for synchronization or channel estimation purposes. In CDMA systems, a pilot signal consisting of a pseudorandom noise (PRN) sequence, known as the short code, is modulated by a carrier signal and broadcast by each BTS for synchronization purposes [31]. Therefore, by knowing the shortcode, the receiver may measure the code phase of the pilot signal as well as its carrier phase, hence forming a pseudorange measurement to each BTS transmitting the pilot signal. In long-term evolution (LTE) systems, two synchronization signals (primary synchronization signal (PSS) and secondary synchronization signal (SSS)) are broadcast by each evolved node B (eNodeB) [32]. In addition to the PSS and SSS, a reference signal known as the cell-specific reference signal (CRS) is transmitted by each eNodeB for channel estimation purposes [32]. The PSS, SSS, and CRS may be exploited to draw carrier phase and pseudorange measurements on neighboring eNodeBs [33,34]. In the rest of this paper, it is assumed that Doppler frequency measurements are available to cellular CDMA or LTE signals (e.g., from specialized navigation receivers [9, 35–38]).

The continuous-time carrier phase observable can be obtained by integrating the Doppler measurement over time [27]. The carrier phase (expressed in cycles) made by the i-th receiver on the n-th SOP is given by

$$\phi_n^{(i)}(t) = \phi_n^{(i)}(t_0) + \int_{t_0}^{t} f_{D_n}^{(i)}(\tau) d\tau, \quad n = 1, \ldots, N, \tag{2}$$

where $f_{D_n}^{(i)}$ is the Doppler measurement made by the i-th receiver on the n-th cellular SOP, $\phi_n^{(i)}(t_0)$ is the initial carrier phase, and N is the total number of SOPs. In (2), the index identifier i denotes either the base (B) or the UAV (U), which are discussed in Subsection III-A. Assuming a constant Doppler during a subaccumulation period T, (2) can be discretized to yield

$$\phi_n^{(i)}(t_k) = \phi_n^{(i)}(t_0) + \sum_{l=0}^{k-1} f_{D_n}^{(i)}(t_l) T, \tag{3}$$

where $t_k \triangleq t_0 + kT$. In what follows, the time argument t_k will be replaced by k for simplicity of notation. Note that the receiver will make noisy carrier phase measurements. Adding measurement noise to (3) and expressing the carrier phase observable in meters yields

$$z_n^{(i)}(k) = \lambda \phi_n^{(i)} + \lambda T \sum_{l=0}^{k-1} f_{D_n}^{(i)}(l) + v_n^{(i)}(k), \tag{4}$$

where λ is the carrier signal wavelength and $v_n^{(i)}$ is the measurement noise, which is modeled as a discrete-time zero-mean white Gaussian sequence with variance $\left[\sigma_n^{(i)}(k)\right]^2$, which can be shown for a coherent second-order phase-locked loop (PLL) to be given by [27]

$$\left[\sigma_n^{(i)}(k)\right]^2 = \lambda^2 \frac{B_{i,\mathrm{PLL}}}{C/N_{0_n}(k)},$$

where $B_{i,\mathrm{PLL}}$ is the receiver's PLL noise equivalent bandwidth and C/N_{0_n} is the cellular SOP's measured carrier-to-noise ratio. Note that a coherent PLL may be employed in CDMA and LTE navigation receivers since the cellular synchronization and reference signals do not carry any data. The carrier phase in (4) can be parameterized in terms of the receiver and cellular SOP states as

$$z_n^{(i)}(k) = \left\| \boldsymbol{r}_{r_i}(k) - \boldsymbol{r}_{s_n} \right\|_2 + c \cdot [\delta t_{r_i}(k) - \delta t_{s_n}(k)] + \lambda N_n^{(i)} + v_n^{(i)}(k), \tag{5}$$

where $\boldsymbol{r}_{r_i} \triangleq [x_{r_i}, y_{r_i}]^{\mathsf{T}}$ is the receiver's position vector; $\boldsymbol{r}_{s_n} \triangleq [x_{s_n}, y_{s_n}]^{\mathsf{T}}$ is the cellular BTS's position vector; c is the speed of light; δt_{r_i} and δt_{s_n} are the receiver's and cellular BTS's clock biases, respectively; and $N_n^{(i)}$ is the carrier phase ambiguity.

III. NAVIGATION WITH SOP CARRIER PHASE DIFFERENTIAL CELLULAR MEASUREMENTS

In this section, a framework for CD-cellular navigation is developed.

A. CD-CELLULAR FRAMEWORK

The framework consists of a navigating UAV and a reference receiver in an environment comprising N cellular BTSs. The UAV and reference receiver are assumed to be listening to the same BTSs with the BTS locations being known. The reference receiver, referred to as the base (B), is assumed to have knowledge of its own position state, e.g., a stationary receiver deployed at a surveyed location. Note that instead of a stationary receiver, the base may be another UAV with access to GNSS and a high-end sensor suite enabling to know its location precisely (e.g., high-flyer). The navigating UAV (U) does not have knowledge of its position nor its velocity. The base communicates its own position and carrier phase observables with the UAV. Fig. 1 illustrates the base/UAV framework.

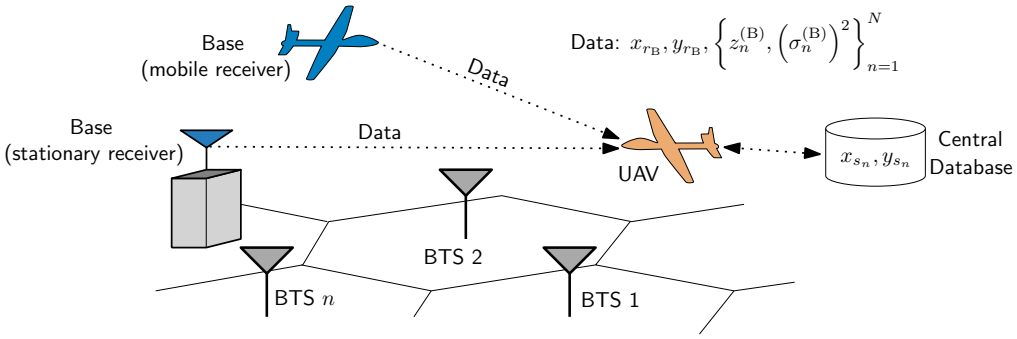

Fig. 1. Base/UAV framework. The base could be either a stationary receiver or another UAV.

In what follows, the objective is to estimate the UAV's position, which will be achieved by double-differencing the measurements (5). Without loss of generality, let the measurements to the first SOP be taken as references to form the single difference

$$z_{n,1}^{(i)}(k) \triangleq z_n^{(i)}(k) - z_1^{(i)}(k).$$

Subsequently, define the double difference between U and B as

$$\begin{aligned} z_{n,1}^{(\mathrm{U,B})}(k) &\triangleq z_{n,1}^{(\mathrm{U})}(k) - z_{n,1}^{(\mathrm{B})}(k) + \|\boldsymbol{r}_{r_\mathrm{B}}(k) - \boldsymbol{r}_{s_n}\|_2 - \|\boldsymbol{r}_{r_\mathrm{B}}(k) - \boldsymbol{r}_{s_1}\|_2 \\ &\triangleq h_{n,1}^{(\mathrm{U})}(k) + \lambda N_{n,1}^{(\mathrm{U,B})} + v_{n,1}^{(\mathrm{U,B})}(k), \end{aligned} \tag{6}$$

where $n = 1, \ldots, N$, ${h_{n,1}}^{(\mathrm{U})}(k) \triangleq \|\boldsymbol{r}_{r_\mathrm{U}}(k) - \boldsymbol{r}_{s_n}\|_2 - \|\boldsymbol{r}_{r_\mathrm{U}}(k) - \boldsymbol{r}_{s_1}\|_2$, $N_{n,1}^{(\mathrm{U,B})} \triangleq N_n^{(\mathrm{U})} - N_n^{(\mathrm{B})} - N_1^{(\mathrm{U})} + N_1^{(\mathrm{B})}$, and $v_{n,1}^{(\mathrm{U,B})}(k) \triangleq v_n^{(\mathrm{U})}(k) - v_n^{(\mathrm{B})}(k) - v_1^{(\mathrm{U})}(k) + v_1^{(\mathrm{B})}(k)$. Define the vector of measurements as

$$\boldsymbol{z}(k) \triangleq \boldsymbol{h}\left[\boldsymbol{r}_{r_\mathrm{U}}(k)\right] + \lambda \boldsymbol{N} + \boldsymbol{v}(k),$$

where

$$\begin{aligned}\boldsymbol{z}(k) &\triangleq \left[z_{2,1}^{(\mathrm{U,B})}(k),\ldots,z_{N,1}^{(\mathrm{U,B})}(k)\right]^{\mathsf{T}}\\ \boldsymbol{h}\left[\boldsymbol{r}_{r_{\mathrm{U}}}(k)\right] &\triangleq \left[h_{2,1}^{(\mathrm{U})}(k),\ldots,h_{N,1}^{(\mathrm{U})}(k)\right]^{\mathsf{T}}\\ \boldsymbol{N} &\triangleq \left[N_{2,1}^{(\mathrm{U,B})},\ldots,N_{N,1}^{(\mathrm{U,B})}\right]^{\mathsf{T}}\\ \boldsymbol{v}(k) &\triangleq \left[v_{2,1}^{(\mathrm{U,B})}(k),\ldots,v_{N,1}^{(\mathrm{U,B})}(k)\right]^{\mathsf{T}},\end{aligned}$$

where $\boldsymbol{v}(k)$ has a covariance $\mathbf{R}_{\mathrm{U,B}}(k)$ which can be readily shown to be

$$\mathbf{R}_{\mathrm{U,B}}(k)=\mathbf{R}^{(1)}(k)+\left\{\left[\sigma_1^{(\mathrm{B})}(k)\right]^2+\left[\sigma_1^{(\mathrm{U})}(k)\right]^2\right\}\boldsymbol{\Xi},$$

where

$$\mathbf{R}^{(1)}(k)\triangleq\mathrm{diag}\left\{\left[\sigma_2^{(\mathrm{B})}(k)\right]^2+\left[\sigma_2^{(\mathrm{U})}(k)\right]^2,\ldots,\left[\sigma_N^{(\mathrm{B})}(k)\right]^2+\left[\sigma_N^{(\mathrm{U})}(k)\right]^2\right\}$$

and $\boldsymbol{\Xi}$ is a matrix of ones.

B. BATCH SOLUTION

The vector $\boldsymbol{N}$ is now a vector of integers and has to be solved for along with the UAV's position. Using only one set of carrier phase measurement with no *a priori* knowledge on the UAV position results in an underdetermined system: $(N+1)$ unknowns with only $(N-1)$ measurements. In GNSS, when no *a priori* information on the position of the UAV (rover) is known, the UAV could remain stationary for a period of time such that enough variation in satellite geometry is observed. Subsequently, the UAV (rover) uses measurements collected at different times in a batch estimator, resulting in an overdetermined system [27]. Other approaches to deal with integer ambiguity resolution for GNSS include [39]. However, cellular SOP transmitters are stationary. Hence, no variation in geometry will be observed unless the navigating UAV is moving. In this case, cellular carrier phase measurements collected at several time-steps could be used in a batch estimator to solve for the positions of the UAV over the different time-steps as well as for the integer ambiguities. Denote K the number of time-steps in which carrier phase measurements are collected to be processed in a batch. Then, the total number of measurements will be $K\times(N-1)$, while the total number of unknowns will be $2K+N-1$. Note that for $N\geq 3$, the resulting system is overdetermined for $K\geq 3$.

Define the collection of measurements from time-step 0 to $K-1$ as

$$\mathbf{z}^K\triangleq\left[\boldsymbol{z}^{\mathsf{T}}(0),\ldots,\boldsymbol{z}^{\mathsf{T}}(K-1)\right]^{\mathsf{T}},$$

which can be expressed as

$$\mathbf{z}^K=\mathbf{h}\left[\mathbf{r}_{r_{\mathrm{U}}}^K\right]+\lambda\bar{\mathbf{I}}^K\boldsymbol{N}+\mathbf{v}^K, \tag{7}$$

$$\mathbf{r}_{r_{\mathrm{U}}}^K\triangleq\begin{bmatrix}\boldsymbol{r}_{r_{\mathrm{U}}}(0)\\ \vdots\\ \boldsymbol{r}_{r_{\mathrm{U}}}(K-1)\end{bmatrix},\quad \mathbf{h}\left[\mathbf{r}_{r_{\mathrm{U}}}^K\right]\triangleq\begin{bmatrix}\boldsymbol{h}\left[\boldsymbol{r}_{r_{\mathrm{U}}}(0)\right]\\ \vdots\\ \boldsymbol{h}\left[\boldsymbol{r}_{r_{\mathrm{U}}}(K-1)\right]\end{bmatrix},\quad \bar{\mathbf{I}}^K\triangleq\begin{bmatrix}\mathbf{I}_{(N-1)\times(N-1)}\\ \vdots\\ \mathbf{I}_{(N-1)\times(N-1)}\end{bmatrix},\quad \mathbf{v}^K\triangleq\begin{bmatrix}\boldsymbol{v}(0)\\ \vdots\\ \boldsymbol{v}(K-1)\end{bmatrix},$$

where $\mathbf{v}^K$ is the overall measurement noise with covariance $\mathbf{R}^K\triangleq\mathrm{blkdiag}\left[\mathbf{R}_{\mathrm{U,B}}(0),\ldots,\mathbf{R}_{\mathrm{U,B}}(K-1)\right]$, where blkdiag is a block-diagonal matrix. A weighted nonlinear least-squares (WNLS) estimator is used to estimate $\mathbf{r}_{r_{\mathrm{U}}}^K$ along with the float solution of $\boldsymbol{N}$. Then, an integer least-squares (ILS) estimator is employed to fix the integer ambiguities $\boldsymbol{N}$ and the estimate of $\mathbf{r}_{r_{\mathrm{U}}}^K$ is subsequently corrected using the fixed ambiguities. However, the WNLS has to be initialized properly such that 1) the measurement Jacobian with respect to the receiver positions is full column-rank and 2) the WNLS converges to the right basin of attraction. In order to provide a proper initialization, an extended Kalman filter (EKF) will be used to estimate $\mathbf{r}_{r_{\mathrm{U}}}^K$ and $\boldsymbol{N}$ for some $K\geq 3$. Next, the EKF estimates are used to initialize the batch WNLS. For $k>K$, the fixed ambiguities are used to estimate the UAV's position $\boldsymbol{r}_{r_{\mathrm{U}}}(k)$. The EKF model is discussed next.

C. EKF MODEL

Define the vector $\boldsymbol{x} \triangleq \left[\boldsymbol{x}_{r_{\mathrm{U}}}^{\mathsf{T}}, \boldsymbol{N}^{\mathsf{T}}\right]^{\mathsf{T}}$ as the state vector to be estimated. Note that at this point, only the float solution of $\boldsymbol{N}$ is estimated. The EKF will produce an estimate $\hat{\boldsymbol{x}}(k|j)$, i.e., an estimate of $\boldsymbol{x}(k)$ using all measurements up to time-step $j \leq k$, along with an estimation error covariance $\mathbf{P}(k|j) \triangleq \mathbb{E}\left[\tilde{\boldsymbol{x}}(k|j)\tilde{\boldsymbol{x}}^{\mathsf{T}}(k|j)\right]$ where $\tilde{\boldsymbol{x}}(k|j) \triangleq \boldsymbol{x}(k) - \hat{\boldsymbol{x}}(k|j)$ is the estimation error. The EKF estimate and covariance time update equations are readily obtained from (1) and are given by

$$\hat{\boldsymbol{x}}(k+1|k) = \mathbf{F}\hat{\boldsymbol{x}}(k|k), \qquad \mathbf{P}(k+1|k) = \mathbf{F}\mathbf{P}(k|k)\mathbf{F}^{\mathsf{T}} + \mathbf{Q},$$
$$\mathbf{F} \triangleq \operatorname{diag}\left[\mathbf{F}_{r_{\mathrm{U}}}, \mathbf{I}_{(N-1)\times(N-1)}\right], \quad \mathbf{Q} \triangleq \operatorname{diag}\left[\mathbf{Q}_{r_{\mathrm{U}}}, \epsilon\mathbf{I}_{(N-1)\times(N-1)}\right],$$

where ϵ is some small positive number that ensures that $\mathbf{Q}$ is positive definite [40,41]. The EKF state and covariance measurement update is performed according to

$$\hat{\boldsymbol{x}}(k+1|k+1) = \hat{\boldsymbol{x}}(k+1|k) + \mathbf{K}\boldsymbol{\nu}(k+1), \qquad \mathbf{P}(k+1|k+1) = [\mathbf{I} - \mathbf{K}\mathbf{H}]\,\mathbf{P}(k+1|k),$$

$$\boldsymbol{\nu}(k+1) \triangleq \boldsymbol{z}(k+1) - \left[\boldsymbol{h}\left[\hat{\boldsymbol{r}}_{r_{\mathrm{U}}}(k+1|k)\right] + \lambda\hat{\boldsymbol{N}}(k+1|k)\right],$$
$$\mathbf{K} \triangleq \mathbf{P}(k+1|k)\mathbf{H}^{\mathsf{T}}\mathbf{S}^{-1},$$
$$\mathbf{S} \triangleq \mathbf{H}\mathbf{P}(k+1|k)\mathbf{H}^{\mathsf{T}} + \mathbf{R}_{\mathrm{U,B}}(k+1),$$

where $\mathbf{H}$ is the measurement Jacobian given by

$$\mathbf{H} \triangleq \left[\mathbf{T}\mathbf{G} \quad \mathbf{0}_{(N-1)\times 2} \quad \mathbf{I}_{(N-1)\times(N-1)}\right], \qquad \mathbf{G} \triangleq \begin{bmatrix} \frac{\hat{\boldsymbol{r}}_{r_{\mathrm{U}}}^{\mathsf{T}}(k+1|k) - \boldsymbol{r}_{s_1}^{\mathsf{T}}}{\left\|\hat{\boldsymbol{r}}_{r_{\mathrm{U}}}(k+1|k) - \boldsymbol{r}_{s_1}\right\|_2} \\ \vdots \\ \frac{\hat{\boldsymbol{r}}_{r_{\mathrm{U}}}^{\mathsf{T}}(k+1|k) - \boldsymbol{r}_{s_N}^{\mathsf{T}}}{\left\|\hat{\boldsymbol{r}}_{r_{\mathrm{U}}}(k+1|k) - \boldsymbol{r}_{s_N}\right\|_2} \end{bmatrix}, \qquad \mathbf{T} \triangleq \left[-\mathbf{1}_{N-1} \quad \mathbf{I}_{(N-1)\times(N-1)}\right],$$

and $\mathbf{1}_{N-1}$ is an $(N-1)\times 1$ vector of ones.

D. EKF INITIALIZATION

In order to initialize the EKF, i.e., obtain $\hat{\boldsymbol{x}}(0|0)$ and $\mathbf{P}(0|0)$, a centroid positioning method is used based on the hearable cell IDs [42]. To this end, the UAV position is initialized at the centroid of the SOP positions, denoted $\boldsymbol{r}_c$. The UAV initial position's 3σ bound is set to be the maximum distance at which the SOP signals can be acquired and tracked reliably by the receiver, which from experimental results was determined to be 7 km. The initial velocity is set to zero and its corresponding 3σ bound is set to be that of the maximum velocity with which the UAV can fly (e.g., specified by the manufacturer's specification sheet). The initial estimate and uncertainty of the float solution of $\boldsymbol{N}$ can be deduced from the initial position estimates and $\boldsymbol{z}(0)$.

IV. SIMULATION RESULTS

In this section, the following aspects of the framework described in Section III are studied through Monte Carlo simulations: 1) the effect of K on the navigation performance and 2) and the effect of N on the navigation performance. A total of 500 Monte Carlo runs were performed and the total position root mean-squared error (RMSE) was calculated for each value of N and K. The BTS layout, the base's position, and a sample UAV trajectory are plotted in Fig. 2. The UAV was set to start at the same initial position indicated in Fig. 2 for all the Monte Carlo runs. The cellular carrier phase measurements were simulated at 1 Hz for both receivers. The total position RMSEs are shown in Fig. 3 for varying values of N and K. Note that the Least-Squares AMBiguity Decorrelation Adjustment (LAMBDA) method [43] implemented at the Delft University of Technology was used to solve for the integer ambiguities [44].

The following can be deduced from Fig. 3. First, it can be readily seen, as expected, that the total RMSE decreases as K and N increase. However, the decrease in RMSE becomes less significant for large values of K and N. For a

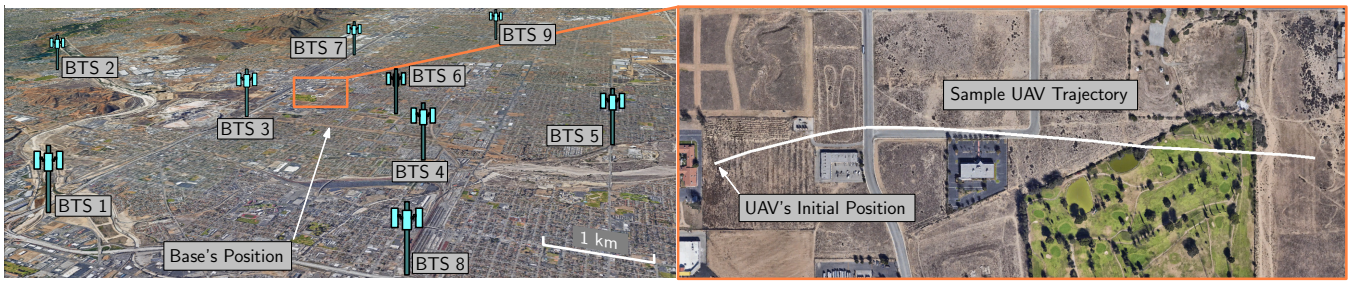

Fig. 2. The BTS layout, the base's position, and a sample UAV trajectory used for 500 Monte Carlo runs.

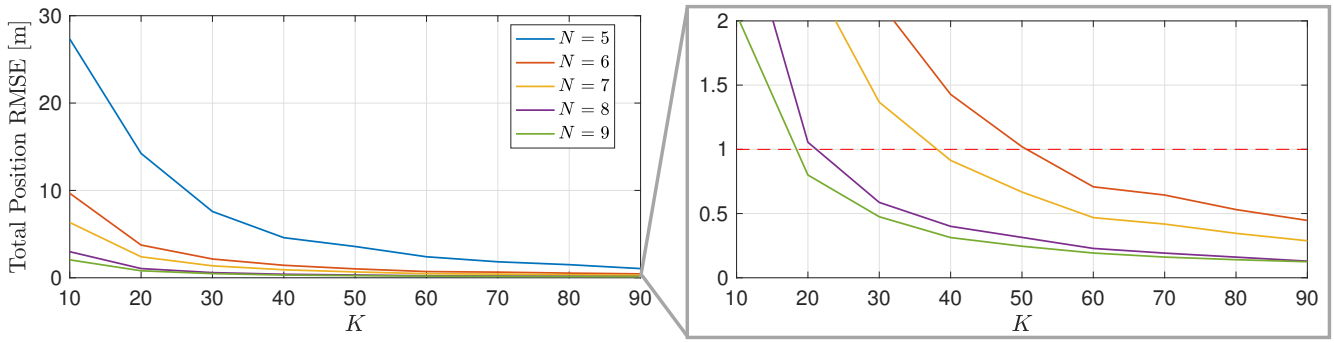

Fig. 3. Total position RMSEs for 500 Monte Carlo runs of the CD-cellular framework described in Section III for varying values of K and N.

given K, the change in the RMSE becomes very small when $N \geq 8$. For a given N, the change in RMSE becomes very small when $K \geq 60$. Subsequently, when 8 or more BTSs are available, little improvement is expected over $K \geq 60$. Second, to achieve centimeter-level performance for a reasonable value of K, e.g., for $K \leq 60$, 6 or more BTSs are needed.

V. CD-CELLULAR NETWORK DESIGN

In this section, preliminary CD-cellular network design considerations and a feasible base architecture are discussed.

A. NUMBER OF BASES AND PLACEMENT

In order to determine the number of bases needed in an area A, the minimum distance d_0 above which received cellular signals become unreliable for navigation must be determined. In this paper, reliable signals are defined as signals received at a C/N_0 above 35 dB-Hz on average [45]. Experimental data collected in a semi-urban environment in Colton, California, shows that d_0 in such environments is 6 km. A C/N_0 plot for 9 cellular BTSs within 6 km of the receiver are shown for a period of 3 minutes in Fig. 4. It can be seen that the C/N_0 is above 35 dB-Hz most of the time for $d_0 = 6$ km. For a true urban environment, it is assumed that the maximum distance is halved. Moreover, a cellular (hexagonal)-type coverage for each base is considered since it was proven efficient in cellular systems. Subsequently, 0.0107 bases/km^2 will be needed in a semi-urban environment and 0.0428 bases/km^2 will be needed in a true urban environment. To put things into perspective, 52 bases will be needed to cover the 1,214 km^2 land area of the city of Los Angeles, California.

B. COMMUNICATION REQUIREMENTS AND SYNCHRONIZATION

The base can produce carrier phase observables from cellular signals at a rate of 100 Hz. In typical navigation systems, pseudorange or carrier phase updates are usually performed at up to 10 Hz. However, even at 100 Hz, these rates can be trivially achieved using today's wireless technology. Moreover, cellular base stations are required to be

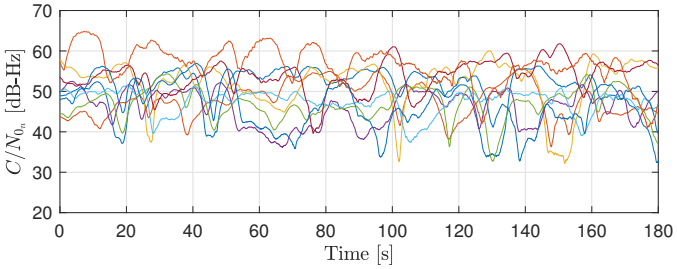

Fig. 4. Carrier-to-noise ratios $\{C/N_{0_n}\}_{n=1}^{9}$ of all the cellular BTSs measured by the UAV. The C/N_0 measured by the base were of similar values.

synchronized to within 10 μs from GPS time. Subsequently, the base and UAV can align the observables in time based on the cellular system time without introducing significant latencies. Accounting for the distances between the base and UAV and each base station, a maximum latency of 60 μs could be observed. This latency is way below the time interval in which navigation observables are being produced and will introduce errors below 8mm in the CD-cellular measurements.

C. SOFTWARE-DEFINED RADIO ARCHITECTURE

The cellular navigation receiver on-board the base is broken up into three main components. The first component is the front-end (FE) abstraction layer (FEAL). The FEAL is primarily responsible for interfacing with the FEs which can be universal software radio peripherals (USRPs). Each type of FE is exposed to the rest of the system as an FE object (FEO), which consists of certain configuration methods. In the exact implementation, the FEO is responsible for configuring the various devices using the data provided in the configuration methods. The FEO creates Sample Frames by reading the sample data from the device. A Sample Frame consists of a vector of complex numbers (the raw in-phase and quadrature (IQ) components) and a sequence number. The next component is the channel bank (CB). A CB performs cellular signal acquisition and tracking, which are spread across two different objects. The CB itself is responsible for conducting acquisition. Once a cellular SOP is acquired, a channel object (CO) is created. A CO contains all the necessary functions and algorithms necessary to track the signal and produce pseudorange and carrier phase observables, which are eventually transmitted to the UAV.

The core architecture of the base consists of an array of Pipeline Objects (POs). A PO consists of a single FEO and a single CB. Data communication between the two objects uses a lockless queue. The data passed between the two objects is a shared pointer to a sample frame object (SFO), which is a set or raw IQ samples. Then, each of the outputs of the pipelines are passed to the communication device that will transmit the observables to the UAV. This architecture is illustrated in Fig. 5.

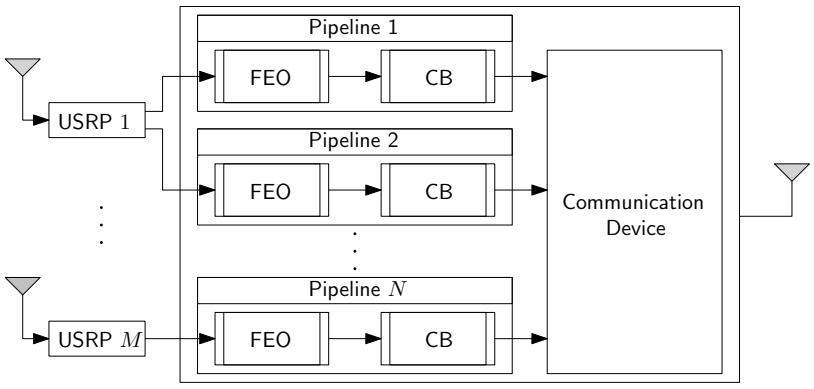

Fig. 5. Base SDR core architecture.

Each object and component described above are implemented as abstract classes in C++, which can be extended into more concrete classes depending on the cellular signal structure. For example, a CB can be extended to a cellular

CDMA CB, in which the tracking and acquisition functions are modified according to [37]. This can be applied to various other objects throughout the base's SDR. This abstracts the specific cellular SOP signal structure from the rest of the receiver architecture. Furthermore, each channel within the CBs, the IQ sample gathering function in the FEO, and the acquisition operation in a CB are set to run in independent threads with different priorities. The IQ sample gathering threads in the FEO are given the highest priority because of the hardware dependence. This means that a "slow" channel implementation will not impact the rest of the receiver. Also, each of the components are decoupled from one another using queues. This allows for simultaneous development of the base's receiver and its components independently of the architecture. This is a result of using queues to communicate data, which represent standard interfaces for each component to interact with.

Due to the relatively large number of hearable SOPs in the base's environment, the base's receiver needs to maintain a high throughput rate. This is achieved using several key technologies. The first is the Single Instruction Multiple Data (SIMD) technology, which effectively allows the same instruction to be performed on multiple pieces of data in a single clock cycle. This is implemented as Advanced Vector eXtensions (AVX) on Intel processors. This allows for multiple samples to be processed simultaneously in a single clock cycle, increasing the throughput tremendously. The SDR could also leverage multicore processors. Due to the highly parallelizable nature of the receiver's architecture, the more cores available to the program, the faster it runs. This is due to the fact that there are generally more threads than there are cores, creating a backlog of threads that require processor time. The number of threads that can be executed in parallel increases as the number of cores increases. The receiver uses highly optimized computing libraries to assist in several calculations. Libraries such as EIGEN and FFTW can easily take advantage of SIMD instructions. In addition, EIGEN is compiled to leverage the use of Intel's Math Kernel Library which contains several high performance matrix and signal processing operations.

VI. EXPERIMENTAL RESULTS

In this section, experimental results are presented demonstrating centimeter-level-accurate UAV navigation results using the CD-cellular framework developed in this paper. As mentioned in Section II, only the 2–D position of the UAV is estimated as its altitude may be obtained using other sensors (e.g., an altimeter). In the following experiments, the altitude of the UAV was obtained from its on-board navigation system. Moreover, the noise equivalent bandwidths of the receivers' PLLs were set to $B_{\mathrm{N,PLL}} = B_{\mathrm{M,PLL}} = B_{\mathrm{PLL}} = 3$ Hz. In order to demonstrate the CD-cellular framework discussed in Section III, two Autel Robotics X-Star Premium UAVs were equipped each with an Ettus E312 USRP, a consumer-grade 800/1900 MHz cellular antenna, and a small consumer-grade GPS antenna to discipline the on-board oscillator. Note that one UAV acted as a base and the other as a navigating UAV. The receivers were tuned to a 882.75 MHz carrier frequency (i.e., $\lambda = 33.96$ cm), which is a cellular CDMA channel allocated for the U.S. cellular provider Verizon Wireless. Samples of the received signals were stored for off-line post-processing. The cellular carrier phase measurements were given at a rate of 37.5 Hz, i.e., $T = 0.0267$ ms. The ground-truth reference for each UAV trajectory was taken from its on-board integrated navigation system, which uses GPS, an inertial measurement unit (IMU), and other sensors. The navigating UAV's total traversed trajectory was 1.72 km, which was completed in 3 minutes. Over the course of the experiment, the receivers on-board the UAVs were listening to 9 BTSs, whose positions were mapped prior to the experiment according to the framework discussed in [46]. A plot of C/N_0 of all the BTSs measured by the UAV is given in Fig. 4. The base measured similar C/N_0 values.

The CD-cellular measurements were used to estimate the navigating UAV's trajectory via the base/UAV framework developed in Section III. The experimental setup, the SOP BTS layout, and the true (from the UAV's on-board integrated navigation system) and estimated (from the proposed CD-cellular) navigating UAV trajectories are shown in Fig. 6. The position RMSE was found to be 62.11 cm over a trajectory of 1.72 km flown over a period of 3 minutes. The LAMBDA method was used to solve for the integer ambiguities [44].

It is important to note that the RMSE was calculated with respect to the trajectory returned by the UAV's on-board navigation system. Although these systems use multiple navigation sensors, they are not equipped with high-precision GPS receivers, e.g., RTK. Therefore, some errors are expected in what is considered to be "true" trajectories taken from the UAV's on-board navigation system. Moreover, the base was mobile during the experiment and the position returned by its on-board navigation system was used as ground-truth. Consequently, any errors in the base's GPS solution would have degraded the navigating UAV's estimate.

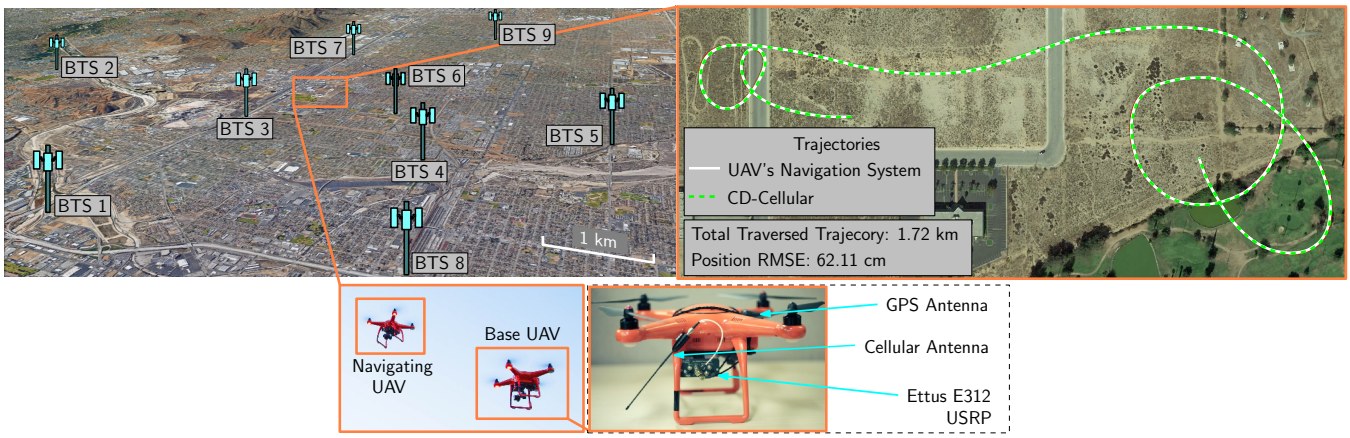

Fig. 6. Experimental setup, the SOP BTS layout, and the true (from the UAV's on-board integrated navigation system) and estimated (from the proposed CD-cellular) navigating UAV trajectories via CD-cellular measurements in the base/UAV framework. The true and estimated trajectories are shown in solid and dashed lines, respectively. Map data: Google Earth.

VII. CONCLUSION

This paper proposed a framework for UAV navigation with CD-cellular measurements. The framework requires no prior knowledge of the UAV's position and achieves centimeter-level accuracy. Monte Carlo simulations were presented to characterize the performance of the proposed framework as a function of the total number of hearable BTSs and the size of the batch estimator. A preliminary study of a CD-cellular network design in terms of number of bases needed, communication and synchronization requirements, and software and hardware considerations for real-time implementation was provided. Experimental results were presented demonstrating a UAV navigating exclusively using the proposed framework over a 1.72 km trajectory completed in 3 minutes with 62.11 cm RMSE.

Acknowledgment

This work was supported in part by the Office of Naval Research (ONR) under Grant N00014-16-1-2305 and in part by the National Science Foundation (NSF) under Grant 1751205. The authors would like to thank Joshua Morales for his help in data collection.

References

[1] J. McEllroy, "Navigation using signals of opportunity in the AM transmission band," Master's thesis, Air Force Institute of Technology, Wright-Patterson Air Force Base, Ohio, USA, 2006.

[2] S. Fang, J. Chen, H. Huang, and T. Lin, "Is FM a RF-based positioning solution in a metropolitan-scale environment? A probabilistic approach with radio measurements analysis," *IEEE Transactions on Broadcasting*, vol. 55, no. 3, pp. 577–588, September 2009.

[3] M. Joerger, L. Gratton, B. Pervan, and C. Cohen, "Analysis of Iridium-augmented GPS for floating carrier phase positioning," *NAVIGATION, Journal of the Institute of Navigation*, vol. 57, no. 2, pp. 137–160, 2010.

[4] K. Pesyna, Z. Kassas, and T. Humphreys, "Constructing a continuous phase time history from TDMA signals for opportunistic navigation," in *Proceedings of IEEE/ION Position Location and Navigation Symposium*, April 2012, pp. 1209–1220.

[5] R. Faragher, C. Sarno, and M. Newman, "Opportunistic radio SLAM for indoor navigation using smartphone sensors," in *Proceedings of IEEE/ION Position Location and Navigation Symposium*, April 2012, pp. 120–128.

[6] J. Khalife, Z. Kassas, and S. Saab, "Indoor localization based on floor plans and power maps: Non-line of sight to virtual line of sight," in *Proceedings of ION GNSS Conference*, September 2015, pp. 2291–2300.

[7] W. Xu, M. Huang, C. Zhu, and A. Dammann, "Maximum likelihood TOA and OTDOA estimation with first arriving path detection for 3GPP LTE system," *Transactions on Emerging Telecommunications Technologies*, vol. 27, no. 3, pp. 339–356, 2016.

[8] A. Tahat, G. Kaddoum, S. Yousefi, S. Valaee, and F. Gagnon, "A look at the recent wireless positioning techniques with a focus on algorithms for moving receivers," *IEEE Access*, vol. 4, pp. 6652–6680, 2016.

[9] K. Shamaei, J. Khalife, and Z. Kassas, "Exploiting LTE signals for navigation: Theory to implementation," *IEEE Transactions on Wireless Communications*, vol. 17, no. 4, pp. 2173–2189, April 2018.

[10] J. Khalife and Z. Kassas, "Navigation with cellular CDMA signals – part II: Performance analysis and experimental results," *IEEE Transactions on Signal Processing*, vol. 66, no. 8, pp. 2204–2218, April 2018.

[11] C. Gentner, T. Jost, W. Wang, S. Zhang, A. Dammann, and U. Fiebig, "Multipath assisted positioning with simultaneous localization and mapping," *IEEE Transactions on Wireless Communications*, vol. 15, no. 9, pp. 6104–6117, September 2016.

[12] P. Muller, J. del Peral-Rosado, R. Piche, and G. Seco-Granados, "Statistical trilateration with skew-t distributed errors in LTE networks," *IEEE Transactions on Wireless Communications*, vol. 15, no. 10, pp. 7114–7127, October 2016.

[13] Z. Kassas, J. Morales, K. Shamaei, and J. Khalife, "LTE steers UAV," *GPS World Magazine*, vol. 28, no. 4, pp. 18–25, April 2017.

[14] Z. Kassas, J. Khalife, K. Shamaei, and J. Morales, "I hear, therefore I know where I am: Compensating for GNSS limitations with cellular signals," *IEEE Signal Processing Magazine*, pp. 111–124, September 2017.

[15] J. Morales, J. Khalife, and Z. Kassas, "GNSS vertical dilution of precision reduction using terrestrial signals of opportunity," in *Proceedings of ION International Technical Meeting Conference*, January 2016, pp. 664–669.

[16] J. Morales, J. Khalife, and Z. Kassas, "Opportunity for accuracy," *GPS World Magazine*, vol. 27, no. 3, pp. 22–29, March 2016.

[17] J. Morales, P. Roysdon, and Z. Kassas, "Signals of opportunity aided inertial navigation," in *Proceedings of ION GNSS Conference*, September 2016, pp. 1492–1501.

[18] J. Morales, J. Khalife, and Z. Kassas, "Collaborative autonomous vehicles with signals of opportunity aided inertial navigation systems," in *Proceedings of ION International Technical Meeting Conference*, January 2017, 805–818.

[19] J. Morales and Z. Kassas, "Distributed signals of opportunity aided inertial navigation with intermittent communication," in *Proceedings of ION GNSS Conference*, September 2017, pp. 2519–2530.

[20] J. Morales and Z. Kassas, "A low communication rate distributed inertial navigation architecture with cellular signal aiding," in *Proceedings of IEEE Vehicular Technology Conference*, 2018, pp. 1–6.

[21] J. Khalife, S. Ragothaman, and Z. Kassas, "Pose estimation with lidar odometry and cellular pseudoranges," in *Proceedings of IEEE Intelligent Vehicles Symposium*, June 2017, pp. 1722–1727.

[22] M. Maaref, J. Khalife, and Z. Kassas, "Lane-level localization and mapping in GNSS-challenged environments by fusing lidar data and cellular pseudoranges," *IEEE Transactions on Intelligent Vehicles*, 2018, accepted.

[23] B. O'Hanlon, M. Psiaki, P. Kintner, and T. Humphreys, "Development and field testing of a DSP-based dual-frequency software GPS receiver," in *Proceedings of ION GNSS Conference*, September 2009, pp. 317–325.

[24] T. Humphreys, J. Bhatti, T. Pany, B. Ledvina, and B. O'Hanlon, "Exploiting multicore technology in software-defined GNSS receivers," in *Proceedings of ION GNSS Conference*, September 2009, pp. 326–338.

[25] C. Fernandez-Prades, J. Arribas, P. Closas, C. Aviles, and L. Esteve, "GNSS-SDR: An open source tool for researchers and developers," in *Proceedings of ION GNSS Conference*, September 2011, pp. 780–794.

[26] F. Principe, G. Bacci, F. Giannetti, and M. Luise, "Software-defined radio technologies for GNSS receivers: A tutorial approach to a simple design and implementation," *International Journal of Navigation and Observation*, 2011.

[27] P. Misra and P. Enge, *Global Positioning System: Signals, Measurements, and Performance*, 2nd ed. Ganga-Jamuna Press, 2010.

[28] E. Kaplan and C. Hegarty, *Understanding* GPS/GNSS*: Principles and applications*, 3rd ed. Artech House, 2017.

[29] J. Khalife and Z. Kassas, "Precise UAV navigation with cellular carrier phase measurements," in *Proceedings of IEEE/ION Position, Location, and Navigation Symposium*, April 2018, pp. 978–989.

[30] X. Li and V. Jilkov, "Survey of maneuvering target tracking. Part I: Dynamic models," *IEEE Transactions on Aerospace and Electronic Systems*, vol. 39, no. 4, pp. 1333–1364, 2003.

[31] 3GPP2, "Physical layer standard for cdma2000 spread spectrum systems (C.S0002-E)," 3rd Generation Partnership Project 2 (3GPP2), TS C.S0002-E, June 2011.

[32] 3GPP, "Evolved universal terrestrial radio access (E-UTRA); physical channels and modulation," 3rd Generation Partnership Project (3GPP), TS 36.211, January 2011. [Online]. Available: http://www.3gpp.org/ftp/Specs/html-info/36211.htm

[33] K. Shamaei, J. Khalife, and Z. Kassas, "Performance characterization of positioning in LTE systems," in *Proceedings of ION GNSS Conference*, September 2016, pp. 2262–2270.

[34] K. Shamaei, J. Khalife, S. Bhattacharya, and Z. Kassas, "Computationally efficient receiver design for mitigating multipath for positioning with LTE signals," in *Proceedings of ION GNSS Conference*, September 2017, pp. 3751–3760.

[35] J. del Peral-Rosado, J. Lopez-Salcedo, G. Seco-Granados, F. Zanier, P. Crosta, R. Ioannides, and M. Crisci, "Software-defined radio LTE positioning receiver towards future hybrid localization systems," in *Proceedings of International Communication Satellite Systems Conference*, October 2013, pp. 14–17.

[36] C. Yang, T. Nguyen, and E. Blasch, "Mobile positioning via fusion of mixed signals of opportunity," *IEEE Aerospace and Electronic Systems Magazine*, vol. 29, no. 4, pp. 34–46, April 2014.

[37] J. Khalife, K. Shamaei, and Z. Kassas, "A software-defined receiver architecture for cellular CDMA-based navigation," in *Proceedings of IEEE/ION Position, Location, and Navigation Symposium*, April 2016, pp. 816–826.

[38] J. Khalife, K. Shamaei, and Z. Kassas, "Navigation with cellular CDMA signals – part I: Signal modeling and software-defined receiver design," *IEEE Transactions on Signal Processing*, vol. 66, no. 8, pp. 2191–2203, April 2018.

[39] B. Pervan and B. Parkinson, "Cycle ambiguity estimation for aircraft precision landing using the Global Positioning System," *Journal of Guidance, Control, and Dynamics*, vol. 20, no. 4, pp. 681–689, July–August 1997.

[40] J. Mendel, *Lessons in Estimation Theory for Signal Processing, Communications, and Control*, 2nd ed. Prentice Hall, 1995.

[41] Y. Bar-Shalom, X. Li, and T. Kirubarajan, *Estimation with Applications to Tracking and Navigation*. New York, NY: John Wiley & Sons, 2002.

[42] N. Bulusu, J. Heidemann, and D. Estrin, "GPS-less low-cost outdoor localization for very small devices," *IEEE Personal Communications*, vol. 7, no. 5, pp. 28–34, October 2000.

[43] P. J. G. Teunissen, "The least-squares ambiguity decorrelation adjustment: a method for fast gps integer ambiguity estimation," *Journal of Geodesy*, vol. 70, no. 1, pp. 65–82, November 1995.

[44] S. Verhagen and B. Li, "LAMBDA software package - MATLAB implementation, version 3.0. Delft Uuniversity of Technology," 2012.

[45] A. J. Van Dierondonck, *Global Positioning System: Theory and Applications*. Washington D.C.: American Institute of Aeronautics and Astronautics, 1996, ch. 8: GPS Receivers, pp. 329–408.

[46] J. Morales and Z. Kassas, "Optimal collaborative mapping of terrestrial transmitters: receiver placement and performance characterization," *IEEE Transactions on Aerospace and Electronic Systems*, vol. 54, no. 2, pp. 992–1007, April 2018.